Chapter 6

Magnetoresistance of Nanowires Electrodeposited into Anodized Aluminum Oxide Nanochannels

Takeshi Ohgai

Additional information is available at the end of the chapter

http://dx.doi.org/10.5772/3367

1. Introduction

One-dimensional nanowires with a large aspect ratio have received much attention due to their unique shape anisotropy and extremely large surface area. Metallic nanowires such as Au, Ag and Cu nanowires [1-3] and semiconductor nanowires [4-9] would show unique electron transport properties which are not observed in bulk metals. Ferromagnetic nanowires such as Ni, Co and Fe alloy nanowires as well as Co/Cu multilayered nanowires would be best candidate materials for magnetic field sensors with anisotropic magnetoresistance (AMR) and giant magnetoresistance (GMR) effect. Nanowires can be fabricated by manipulating metallic atoms one by one using scanning tunneling microscopy (STM) or catalyst-assisted wet chemical etching technique [10], while they can be also prepared by electrochemically depositing metallic atoms into a nanochannel template with numerous nanochannels [11]. Nanochannel templates such as polycarbonate membrane films or anodized aluminum oxide films with high density of nanochannels (about 10^8~10^{10} cm^{-2}) can be used in the template synthesis technique [12].

Using polymer membrane filters, ferromagnetic metal nanowires have been synthe sized so far. Whitney *et al.* reported that the arrays of Ni and Co nanowires were electrodeposited in polymer templates with the nanometer-sized pores prepared by nuclear track etching technique [13]. They found that the preferred magnetization direction is perpendicular to the film plane and enhanced coercive force as high as 680 Oe. Piraux *et al.* reported that the array of Co/Cu multilayered nanowires with GMR response was electrodeposited in nanoporous polymer template [14]. Blondel *et al*. also reported that Co/Cu and Ni-Fe/Cu multilayered nanowires with GMR response was demonstrated [15]. They synthesized the multilayered nanowires with length of 6 μm, diameter of 80 nm and each layer thickness of 5~10 nm into the nanochannels of ion track-etched polycarbonate membrane filters. In the

report, GMR of 14% for Co/Cu and of 10% for Ni-Fe/Cu was demonstrated at ambient temperature in the current perpendicular to the layers. Ohgai *et al.* reported that magneto-sensitive nickel nanowires with AMR response could be fabricated into multi- and single-ion track templates with nanochannels using electrode position technique [16,17].

On the contrary, using anodized aluminum oxide pores on the surface of metallic aluminum substrates, Ni, Co and Fe homogeneous ferromagnetic nanowires have been also electrodeposited and characterized in terms of their magnetization properties. Kawai *et al*. reported that magnetic properties of Ni, Co, Fe, Co-Ni, Fe-Ni and Fe-Co alloy nanowires with the coercive force ranging from 0.5 to 3.2kOe were electrodeposited into the nanopores of an anodic oxide coating films on aluminum [18-20]. Tsuya *et al.* also reported that the alumite films containing Fe nanowires were fabricated as an application to perpendicular magnetic recording medium [21,22]. Huysmans *et al*. reported that the magnetization curling process in perpendicular direction was investigated using Fe nanowire arrays in alumite media [23]. Cheng *et al.* also reported that the magnetic anisotropy of electrodeposited Co nanowires on alumite substrate [24]. Zhang *et al* . reported that the influence of the packing density on the magnetic behaviour was investigated using alumite media containg magnetic nanowires [25]. AlMawlawi *et al*. reported that the coercive force of Fe nanowires electrodeposited into anodic aluminum oxide pores increased up to around 2.1 kOe with increasing the aspect ratio of the nanowires [26]. Nielsch *et al*. reported that the uniform Ni nanowires array was synthesized into the ordered alumina pores by pulsed electrodeposition technique [27]. Evans *et al*. reported that the current perpendicular to plane giant magnetoresistance (CPP-GMR) was found using the multilayered nanowires electrodeposited in a commercially available anodic aluminum oxide membrane filter [28]. Ohgai *et al*. reported that the Co/Cu multilayered nanowires with spin-valve effect and GMR response were synthesized in self-organized anodized aluminum oxide nanopores grown at the surface of bulk aluminum. They also reported that the pore bottom oxide layer was removed by a chemical etching technique using aluminum oxide template with pore-length as short as 2000 nm. In their report, 20% of GMR was demonstrated in Co/Cu multilayered nanowires at room temperature, while the typical resistance switching of spin-valves was also demonstrated in Co/Cu/Co tri-layered nanowires [29-32]. Wu *et al*. reported that the Ni nanodot and nanowire arrays could be prepared using a porous alumina layer on a bulk silicon as a template without a conductive interlayer [33]. Chu *et al*. reported that the integrated ultra high-density Fe-Pt alloy nanowires array was synthesized in a porous alumina layer on an ITO-glass template [34]. Wang *et al*. reported that the Ni nanowires with different diameters were prepared by direct-current electrodeposition into the pores of porous anodic alumina membrane [35]. Friedman *et al*. reported that the optimal parameters were found for synthesis of magnetic nanowires in porous alumina templates [36].

Electrodeposition of metallic nanowires into the as anodized aluminum template can be carried out using an alternating current or a pulsed current in order to reduce the charging up effect of the barrier layer at the interface between the anodized aluminum oxide layer and the metallic aluminum substrate. However, this resistive barrier layer makes it difficult to achieve good electric contacts at the pore bottom and well-controlled layered structure of electrodeposited nanowires. In this chapter, fabrication process of anodized aluminum ox-

http://dx.doi.org/10.5772/3367

ide template without the barrier layer and the magnetoresistance properties of electrodeposited Ni, Co alloy nanowires and Co/Cu multilayered nanowires were investigated to synthesize novel functional ferromagnetic devices with anisotropic magnetoresistance (AMR) effect and giant magnetoresistance (GMR) effect.

2. Fabrication of Anodized Aluminum Oxide Nanochannels Templates

2.1. Barrier Layer Thinning by Chemical Etching Technique

Aluminum sheets with thickness of 500 μm were used as a starting material to prepare anodized aluminum templates. First, the aluminum sheets were electrochemically polished in a ethanol solution containing 25 vol% of perchloric acid to achieve a mirror like surface. During the electrochemical polishing, the cell voltage was kept at 8 V for 10 min at room temperature. Then, the polished aluminum sheets were anodized in an aqueous solution containing 0.3 mol/L oxalic acid to obtain a nanoporous aluminum oxide layer on the surface. During the anodization, the cell voltage was kept at 50 V for 10 min at room temperature. Subsequently, the anodized aluminum sheets were immersed in an aqueous solution containing 5 vol% of phosphoric acid for 50 min to widen the pores, and to thin the oxide layer at the pore bottom. These processing parameters give pores 2 μm long with a diameter of 60 nm.

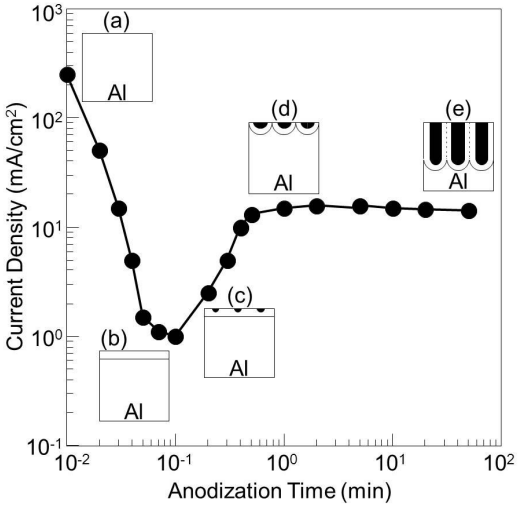

Figure 1. Time dependence of current density on fabrication of self-organized nanoporous anodized aluminum templates. Anodization was conducted under 50 V in aqueous solution containing 0.3 mol/L oxalic acid.

Figure 1 shows the time dependence of current density on the fabrication of self-organized nanoporous anodized aluminum templates. Anodization was conducted under 50 V in aqueous solution containing 0.3 mol/L oxalic acid. At the beginning of anodization, the current density is very high due to oxygen evolution at the surface of aluminum as shown in Figure 1(a). Then, the current density rapidly decreases due to the formation of a highly resistive oxide layer as shown in Figure 1(b). Next, the current density gradually increases due to self-organized formation of nanopores in the oxide layer as shown in Figures 1(c), (d). Finally, the current density reaches a constant value due to a stable growth rate of the porous oxide layer as shown in Figure 1(e).

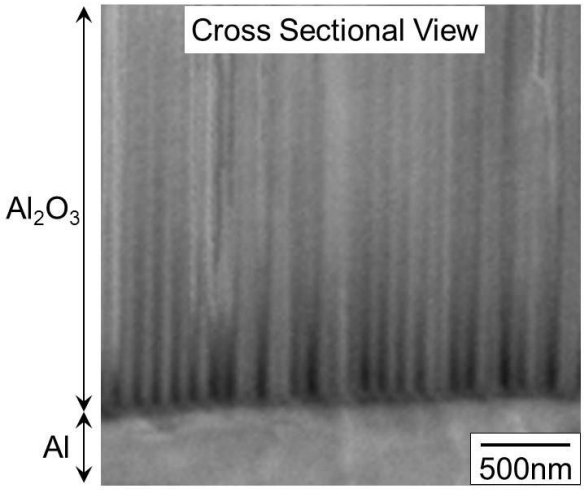

Figure 2. SEM image of a cross section view of an anodized aluminum template. Anodization was conducted under 50 V for 10 min. The anodized aluminum oxide layer has a typical porous columnar structure and the pore length is approximately 2μm. The pore diameter is approximately 60 nm.

Figure 2 shows SEM images of a cross section view of an anodized aluminum template. The oxide layer has a typical porous columnar structure and the pore length is approximately 2μm as shown in Figure 2. The pore diameter is approximately 60 nm and the order of pore density is 10^{10} pores/cm^2 as shown in Figure 2. It is well known that an anodized aluminum template has a resistive oxide layer (barrier layer) at the interface between the anodized aluminum oxide film and the metallic aluminum substrate. Figure 3 shows SEM images of a pore top planar view (a) and a pore bottom back side view (b) of an anodized aluminum template. For observation of pore bottom back side (barrier layer), the massive metallic aluminum substrate was dissolved in hydrochloric acid containing traces of cupric ions. The pore diameter is approximately 60 nm and the order of pore density is 10^{10} pores/cm^2 as shown in Figure 3(a). The existence of a barrier layer is made obvious by looking at the pore bottom of anodized aluminum oxide layer (Figure3(b)).This resistive barrier layer makes

http://dx.doi.org/10.5772/3367

well-controlled electrodeposition of layered structures difficult and lowers their AMR and GMR performance. Electrodeposition of metals into the pores of an anodized aluminum surface is usually carried out using alternating current or a pulsed current technique [37–40] in order to reduce the charging up effect of the barrier layer. To remove this barrier layer, the massive metallic aluminum backing is usually dissolved in an aqueous solution containing $HgCl_2$ prior to thinning the barrier layer [41–45]. However, this aluminum substrate dissolving technique can be applied to thick aluminum oxide layers with the thickness of several tens micro meters. On the contrary, when this barrier layer is removed or thinned without removing the aluminum backing, anodized aluminum templates with short pores length can be obtained. Since the thickness of the barrier layer is about several tens of nanometres, this layer can be removed or thinned using a chemical etching technique from the pore side direction [46]. Therefore, after the anodization process, to remove or thin this barrier layer without dissolving the metallic aluminum backing, the anodized aluminum templates were subsequently immersed in an aqueous solution containing phosphoric acid prior to the electrode position process.

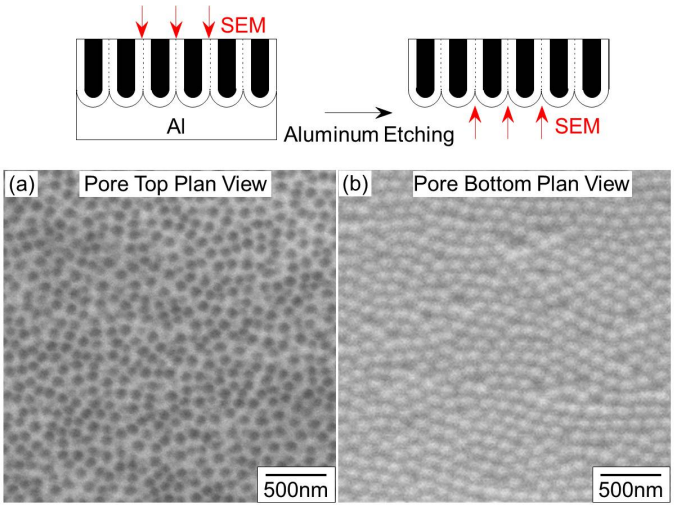

Figure 3. SEM images of pore top plan view (a) and pore bottom plan view (b) of an anodized aluminum template. Anodization was conducted under 50 V for 10 min. The metallic aluminum substrate was dissolved in the hydrochloric acid aqueous solution containing small amount of cupric ions.

2.2. Barrier Layer Thinning by Anodization Voltage Controlling

Figure 4 shows experimental apparatus and time-dependence of applied voltage to synthesize an anodized aluminum oxide membrane filter. Anodized aluminum oxide thick films with numerous nanochannels were exfoliated mechanically by the pressure of hydrogen gas generated at the interface between an oxide layer and a metallic aluminum during the subsequent cathodic reduction process after the growing of anodic aluminum oxide layer. At first,

70 V was applied to growing aluminum oxide long nanochannel. Then, the anodization voltage was decreased gradually down to 0 V for thinning the pore bottom oxide layer (barrier layer). Finally, cathodic voltage was applied to exfoliate an anodized aluminum oxide membrane film from the metallic aluminum rod due to the hydrogen evolution. Figure 5 shows surface appearance of anodized aluminum oxide membrane filters exfoliated from a metallic aluminum rod. These membrane filters were obtained by anodizing at 50 V (Figure 5(a)) and 70 V (Figure 5(b)). The membrane filter anodized at 70 V had round and disc shape with the diameter of 10 mm (Figure 5(b)) while that anodized at 50 V had several cracks (Figure 5(a)).

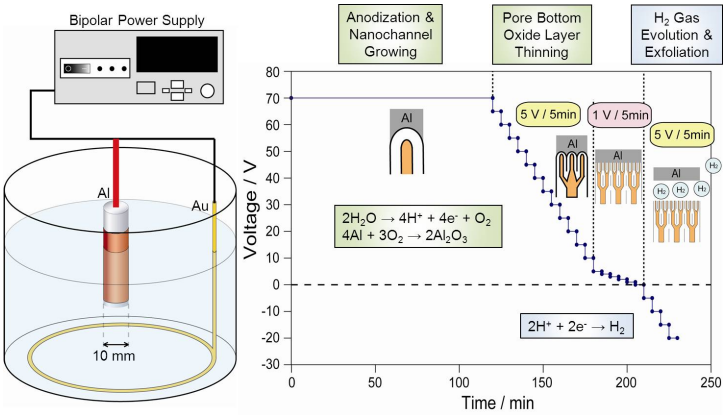

Figure 4. Experimental apparatus and time-dependence of applied voltage to synthesize an anodized aluminum oxide membrane filter.

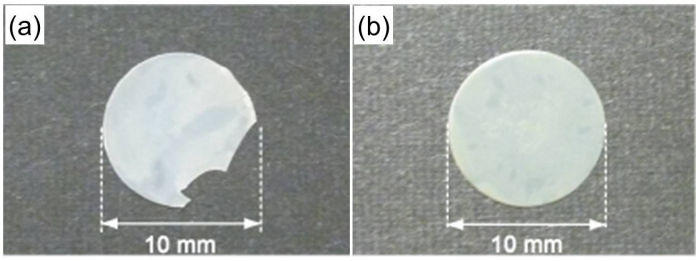

Figure 5. Surface appearance of anodized aluminum oxide membrane filters exfoliated from a metallic aluminum rod. These membrane filters were anodized at 50 V (a) and 70 V (b).

Figure 6 shows SEM images of barrier layer side (plan view (a), cross section (b)) and surface side (plan view (c), cross section (d)) of an anodized aluminum oxide membrane filter exfoliated from a metallic aluminum rod. The anodization was conducted at 70 V. The average channel diameter at the surface side was around 60 nm while that at the barrier layer

http://dx.doi.org/10.5772/3367

side was ca. 20 nm. The oxide layer has a typical porous columnar structure and the channel length was ca. 60 μm while the channel density was around 10^8 channels / cm^2.

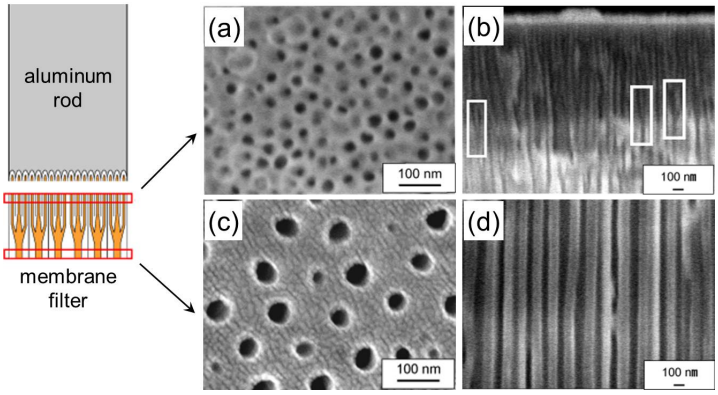

Figure 6. SEM images of barrier layer side (plan view (a), cross section (b)) and surface side (plan view (c), cross section (d)) of an anodized aluminum oxide membrane filter exfoliated from a metallic aluminum rod. The anodization was conducted at 70 V.

Figure 7 shows the effect of anodization voltage on the growth rate of anodized aluminum oxide layer. The oxide layer thickness was determined by observing the cross sectional SEM images. With increasing the anodization voltage V_A(V), the oxide layer thickness was increased exponentially. The average growth rate R_G^{Ave}(nm/sec) of anodized aluminum oxide layer can be expressed by the following equation (1).

$$logR_G^{Ave} = 0.017V_A - 0.34 \quad (1)$$

According to the equation (1), if V_A equal to 70 V, R_G^{Ave} is estimated to be around 7.1 nm/s. Ohgai *et al*. [31] have reported that the average growth rate of the anodized aluminum oxide layer depends on the anodization voltage and the growth rate $R^*_G{}^{Ave}$ (nm/sec) increases exponentially with increasing the anodization voltage V_A (V) as shown in the following equation (2).

$$logR^*_G{}^{Ave} = 0.03V_A - 0.78 \quad (2)$$

According to the equation (2), if V_A equal to 70 V, $R^*_G{}^{Ave}$ is calculated to be around 21 nm/s which is ca. 3 times larger than that obtained from the equation (1). It is well known that the real time growth rate of the anodized aluminum oxide layer R_G^{Real} decreases with increase in the oxide layer thickness. In the equation (1), range of the oxide layer thickness is from 50 to 200 μm while the range is from 1 to 60 μm in the equation (2). Therefore, R_G^{Ave}calculated from the equation (1) would be smaller than that obtained from the equation (2). [1]

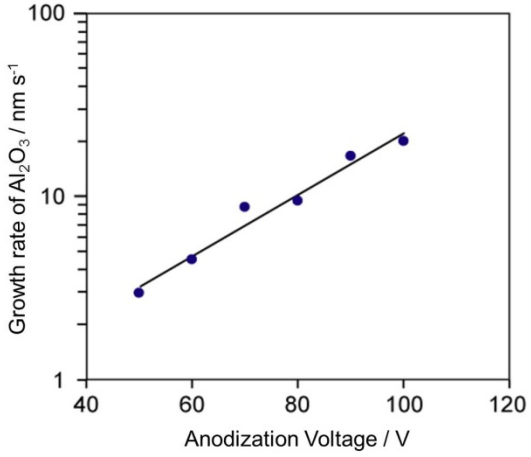

Figure 7. Effect of anodization voltage on the growth rate of anodized aluminum oxide layer.

Figure 8 shows the relationship between film thickness of anodized aluminum oxide layer and anodization time. The anodization was conducted at 70 V. The film thickness y (μm) increased with increasing the anodization time x (hour) according to a parabolic low as shown in the following equation (3).

$$y = 44.7x^{0.47} \tag{3}$$

Therefore, the real time growth rate of the anodized aluminum oxide layer R_G^{Real} can be expressed by the following equation(4).

$$R_G^{Real} = dy/dx = 21.2x^{-0.53}(\text{mm/hour}) = 5.9x^{-0.53}(\text{nm/sec}) \tag{4}$$

Consequently, R_G^{Real} decreases with increase in the anodization time x and the oxide layer thickness y. Ohgai *et al*. [30] have reported that the film thickness y^*(μm) of anodized aluminum oxide layer increases linearly with increasing the anodization time x (hour) as shown in the following equation (5).

$$y = 50x \tag{5}$$

Therefore, the real time growth rate of the anodized aluminum oxide layer $R^*_G{}^{Real}$ would be constant as shown in the following equation (6).

http://dx.doi.org/10.5772/3367

$$R^{*}_{G}{}^{Real} = dy/dx = 50(\text{mm/hour}) = 14(\text{nm/sec}) \quad (6)$$

As mentioned previously, the real time growth rate of the anodized aluminum oxide layer $R_{G}{}^{Real}$ decreases with increase in the oxide layer thickness. In the equation (4), range of the oxide layer thickness is from 50 to 200 μm while the range is from 0.2 to 50 μm in the equation (6). Therefore, $R_{G}{}^{Real}$calculated from the equation (4) would be smaller than that obtained from the equation (6).

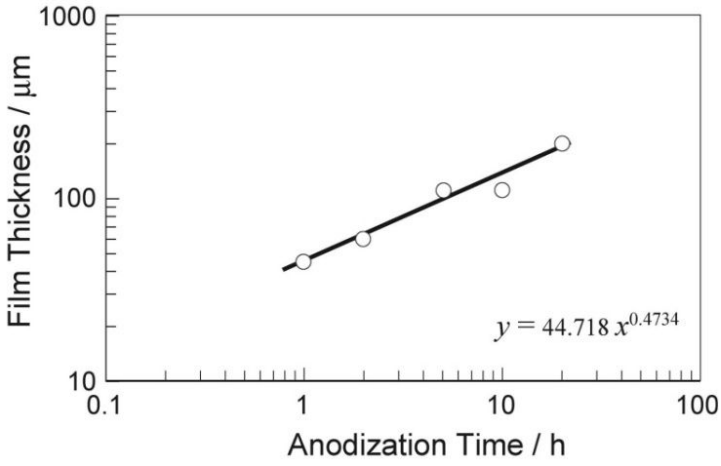

Figure 8. Relationship between film thickness of anodized aluminum oxide layer and anodization time. The anodization was conducted at 70 V.

3. Electrodeposition and Magnetoresistance of Ni and Co Nanowires Array

3.1. Electrodeposition of Ni and Co Nanowires Array

Figure 9 shows experimental apparatus and a nanochannel template for electrodeposition of nanowires array. The exfoliated anodized aluminum oxide nanochannels were used as templates for growing nanowires. On surface of the membrane filter, a gold layer was sputter-deposited to cover the pores and make a cathode. A gold wire and Ag/AgCl electrode were used as an anode and a reference electrode. For example, aqueous solution containing $NiSO_4$ (120 g/L) and H_3BO_3 (45 g/L) was used as electrolyte for electrodeposition of Ni nanowires.

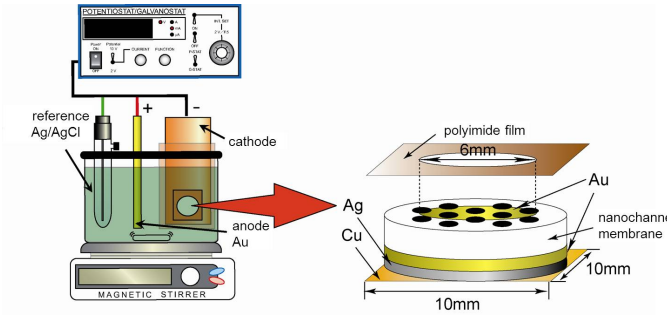

Figure 9. Experimental apparatus and a nanochannel template for electrodeposition of nanowires array.

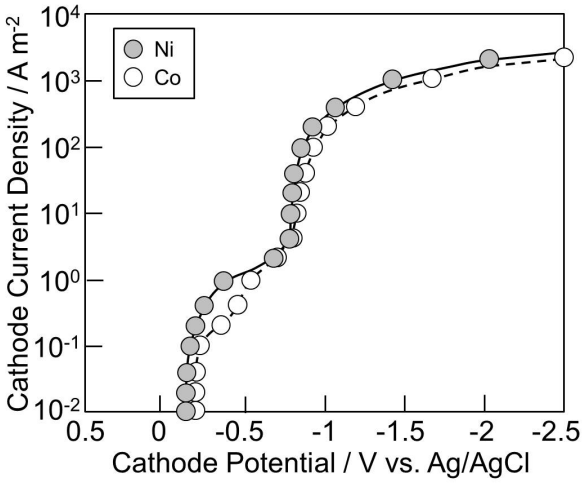

Figure 10. Cathode polarization curves for Ni and Co electrodeposition from aqueous solution containing Ni^{2+} or Co^{2+} ions.

Figure 10 shows cathode polarization curves for Ni and Co electrodeposition from aqueous solution containing Ni^{2+} or Co^{2+}ions. According to Nernst equation, the equilibrium potentials of Ni/Ni^{2+} and Co/Co^{2+} are estimated to be around −0.46 and −0.48V (vs. Ag/AgCl). As shown in Figure 10, the cathodic currents occur at around -0.2V which is more nobler potential region than the equilibrium potential of Ni and Co. Therefore, this cathodic current would be mainly caused by the reduction current of hydrogen ions. With increasing the cathodic current density, at around $2A/m^2$, the potential polarizes significantly to the less noble region. This polarization would be caused by the diffusion limit of hydrogen ions. At around -0.8V which is less nobler potential region than the equilibrium potential of Ni and Co, the cathodic current increases again. It is well-known that the electrodeposition of iron-

group metals such as Ni, Co and Fe is accompanied by the over potential due to the rate determination of multi-step reduction process even in the form of their aqua ions. Therefore, in the present work, Ni^{2+} and Co^{2+} ions would electrodeposit with accompanying the over-potential even in simple aqueous solutions containing sulfuric and boric acid. Consequently, this cathodic current would be mainly caused by the reduction current of Ni^{2+} and Co^{2+}. These characteristics are identical to those obtained with the pores in nanochannel polycarbonate templates with metallic gold cathode. This result supports the observation that the barrier layer at the pore bottom of an anodized aluminum template is well removed by the exfoliation process from a metallic aluminum rod and the nanowires growon metallic gold cathode. Using the polarization curves, the optimum electrodeposition potential range for growing Ni and Co nanowires are determined to be from −1.0 to -1.2V (vs. Ag/AgCl) which is the potential region more nobler than the diffusion limit of each metal ions.

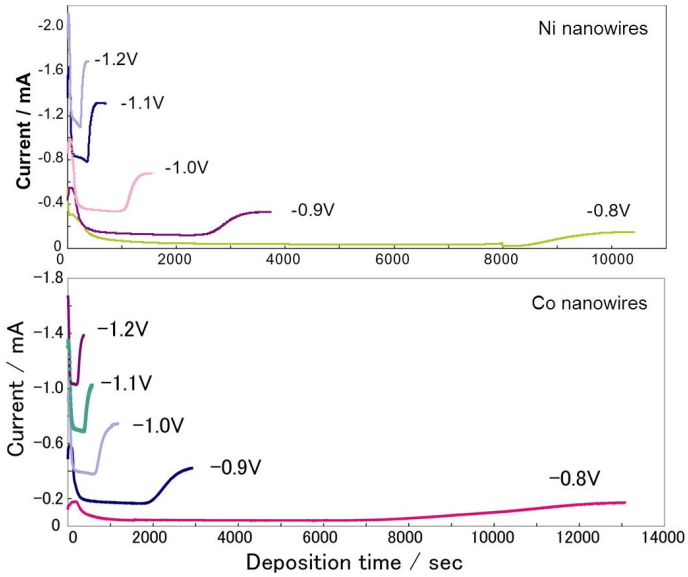

Figure 11. Effect of cathode potential on the time-dependence of cathode current during the electrodeposition of Ni nanowires and Co nanowires.

Time dependence of cathode current was monitored during the electrodeposition to investigate the growing process of nanowires. Ni nanowires and Co nanowires were potentio-statically electrodeposited. Figure 11 shows the effect of cathode potential on the time-dependence of cathode current during the electrodeposition of Ni nanowires and Co nanowires. During the electrodepostion, cathode potentials were fixed to -0.8, –0.9, –1.0, –1.1 and –1.2 V. If the potential was kept to –1.0 V for Ni deposition, the cathode current reached up to ca. 1 mA at the beginning of electrolysis within several tens of minutes. Then, the current rapidly decreased to be ca. 0.4 mA and kept the constant current until around 1000 sec.

During this process, electrodeposition of Ni proceeds in the nanopores. At the initial stage of the electrodepostion, large cathode current was observed in each cathode potential. The concentration of metal ions in the nanopores will decrease with increasing the electrodeposition time due to the reduction of metal ions, while the metal ions will be provided from the bulk solution to the nanopores, where the metal ions are consumed on the cathode due to the electrodeposition process. Finally, as shown in Figure 11, the cathode current rapidly increases at the deposition time more than 1000 sec. At this stage, electrodeposited nanowires reach the surface of the membranes and large hemispheric Ni deposits are formed. Growth rate of Ni nanowires can be estimated from dividing channel length by the filling time. For example, growth rate of Ni nanowires can be estimated as ca. 6 nm/sec at the cathode potential of –1.0 V. Time-dependence of cathode current for Co deposition also showed similar behavior as well as Ni deposition. Growth rate of the nanowires increases up to ca. 30nm/sec with increasing the cathode potential up to -1.2 V.

3.2. Structure of Ni and Co Nanowires Array

After the growing nanowires, anodized aluminum oxide membrane filters were dissolved in aqueous solution containing sodium hydroxide and the remains consisted of nanowires and a gold layer was served as a sample for scanning electron microscope (SEM) and transmission electron microscope (TEM) observation. Figure 12 shows SEM images of Ni nanowires separated from the anodized aluminum oxide templates. Diameter (60 and 300 nm) and length (6 and 30μm) of the nanowires corresponds well to that of nanopores and the cylindrical shape was precisely transferred from the nanopores to the nanowires. Aspect ratio of the nanowires reaches up to around 100.

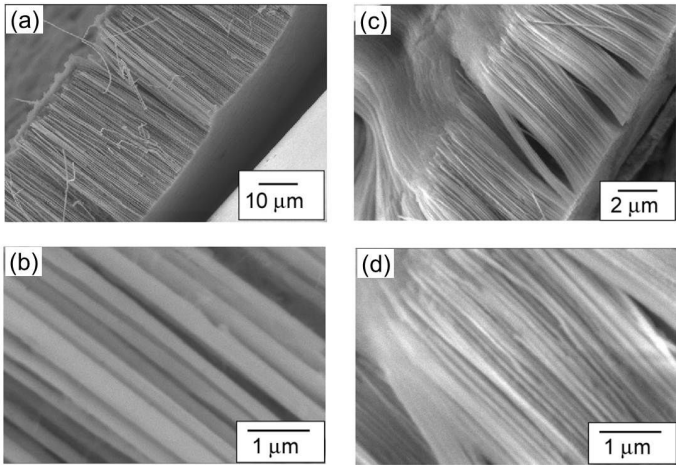

Figure 12. SEM images of electrodeposited Ni nanowires separated from anodized aluminum oxide membrane filters with the pore diameters of ca. 300nm (a),(b) and ca. 60nm (c),(d).

http://dx.doi.org/10.5772/3367

TEM bright field images and electron diffraction patterns of electrodeposited Ni and Co nanowires were also investigated as shown in Figure 13. According to TEM bright field images, shape of the nanowires was almost cylindrical and the electron diffraction patterns are composed of spots, which suggests a nanowire consists of a crystalline phase with preferential orientation.

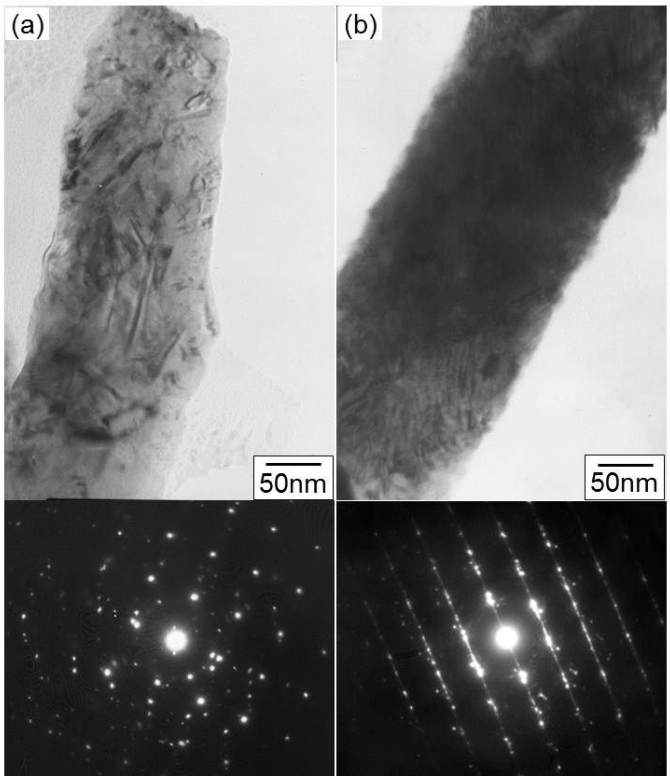

Figure 13. TEM bright field images and electron diffraction patterns of Ni and Co nanowires electrodeposited in nanochannel membrane filters.

3.3. Magnetic Properties of Ni and Co Nanowires Array

Magnetization and anisotropic magnetoresistance (AMR) of Ni alloy and Co alloy nanowires were measured using a vibrating sample magnetometer (VSM) and LCR meter with increasing the magnetic field up to 10 kOe. Figure 14 shows magnetic hysteresis loops of pure Ni, Ni-1.5%Co, Ni-0.8%Fe, pure Co, Co-0.9%Ni and Co-0.1%Fe alloy nanowires electrodeposited into anodized aluminum oxide templates with channel-diameter of 60 nm. Magnetic field was applied to in-plan direction and perpendicular direction to the mem-

brane film plan. The perpendicular direction to the membrane film plan corresponds to the parallel direction to the long axis of nanowires. These nanowires were hardly magnetized in in-plan direction and the magnetization reached to saturation at more than 5 kOe as shown in Figure 14. On the contrary, these nanowires were easily magnetized in perpendicular direction and the coercive force reached up to around 1 kOe. These magnetization curves revealed that the electrodeposited nanowires have a typical perpendicular magnetization behaviour due to the uni-axial shape anisotropy.

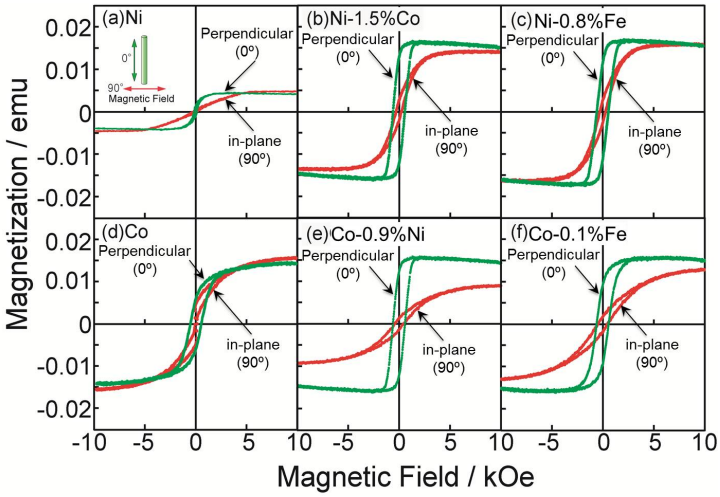

Figure 14. Magnetic hysteresis loops of pure Ni, Ni-1.5%Co, Ni-0.8%Fe, pure Co, Co-0.9%Ni and Co-0.1%Fe alloy nanowires electrodeposited into anodized aluminum oxide templates with channel-diameter of 60 nm. Magnetic field was applied to in-plan direction and perpendicular direction to the membrane film plan. The perpendicular direction to the membrane film plan corresponds to the parallel direction to the long axis of nanowires.

Figure 15 shows magnetoresistance curves of pure Ni, Ni-1.5%Co, Ni-0.8%Fe, pure Co, Co-0.9%Ni and Co-0.1%Fe alloy nanowires electrodeposited into anodized aluminum oxide templates with channel-diameter of 60 nm. Magnetic field was applied to in-plan direction and perpendicular direction to the membrane film plan. The perpendicular direction to the membrane film plan corresponds to the parallel direction to the long axis of nanowires. Here, the anisotropic magnetoresistance (AMR) ratio is defined by the following equation:

$$\mathrm{AMR}(\%) = 100 \times (\mathrm{R_{max}} - \mathrm{R_{min}}) / \mathrm{R_{min}} \tag{7}$$

The magnetoresistive hysteresis of the Ni alloy and Co alloy nanowires depended strongly on the direction of the magnetic field as shown in Figure 15. In the magnetic field direction of 0° (the long axis of nanowires is parallel to the magnetic field), the AMR ratio was almost zero, while a maximum AMR ratio was observed in the magnetic field direction of 90° (the long axis of nanowiresis perpendicular to the magnetic field). Resistance of the nanowires

http://dx.doi.org/10.5772/3367

decreased with increase in the magnetic field and the AMR ratio reached 1.0–3.2% with the Ni alloy nanowires. The saturation field of the Ni nanowires was estimated to be about 7 kOe. Ferre *et al.* [47] reported on the magnetoresistance of Ni and Co nanowires electrodeposited in ion-track etched polycarbonate templates. In their report, the magnetoresistance curves obtained from Ni nanowires showed typical AMR behaviour (1.4% of AMR ratio) over a wide range of the diameter in the nanowires, which corresponds well with the results obtained in this study. On the contrary, AMR ratio of the Co alloy nanowires was only 0.6–0.8%. The range of applied magnetic fields was not enough to measure the saturation magnetic field of Co nanowires. Since the magnetic field was insufficient to saturate the magnetization of Co nanowires, the AMR value was not actual full value.

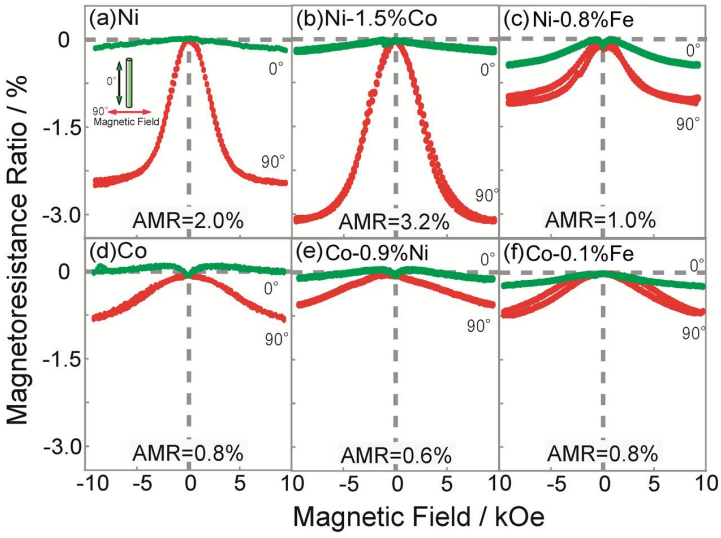

Figure 15. Magnetoresistance curves of pure Ni, Ni-1.5%Co, Ni-0.8%Fe, pure Co, Co-0.9%Ni and Co-0.1%Fe alloy nanowires electrodeposited into anodized aluminum oxide templates with channel-diameter of 60 nm.Magnetic field was applied to in-plan direction and perpendicular direction to the membrane film plan. The perpendicular direction to the membrane film plan corresponds to the parallel direction to the long axis of nanowires.

4. Electrodeposition and Magnetoresistance of Co/Cu Multilayered Nanowires

4.1. Electrodeposition of Co/Cu Multilayered Nanowires

For growing Co/Cu multilayered nanowires, the exfoliated anodized aluminum oxide nanochannels were used as templates. Aqueous solution containing $CoSO_4$ (120 g/L), $CuSO_4$ (1.6 g/L) and H_3BO_3 (45 g/L) was used as electrolyte for electrodeposition of Co/Cu multilayered

nanowires. A cathode polarization curve was measured over a wide range of cathode potential to determine the optimum potential for Cu and Co deposition. Figure 16 shows cathode polarization curves for electrodeposition of Cu and Co from the mixed solution (containing Cu^{2+} and Co^{2+} ions) and the solution containing only Co^{2+} ions. The equilibrium potentials of Cu/Cu^{2+} and Co/Co^{2+} are estimated to be around +0.05 V and –0.48 V (vs.Ag/AgCl) on the basis of Nernst equation.The cathode current occurs at the potential region close to the equilibrium potential of Cu as shown in Figure 16. It is well-known that Cu^{2+} ions begin to electrodeposit without accompanying overpotential from the aqueous solution. Therefore, this cathode current corresponds to the deposition current of Cu. With increasing cathode current, at around 10^{-2}A, the potential significantly polarizes to the less-noble region. This polarization would be caused by the diffusion limit of Cu^{2+} ions. In the potential region which is less-nobler than the equilibrium potential of Co, the cathode current increases again at around –0.7 V. It is also well-known that the electrodeposition of iron-group metals such as Ni, Co, and Fe is accompanied by the overpotential due to the rate determination of multistep reduction process. Therefore, this increase in cathode current would be mainly caused by the reduction current of Co^{2+} ions.

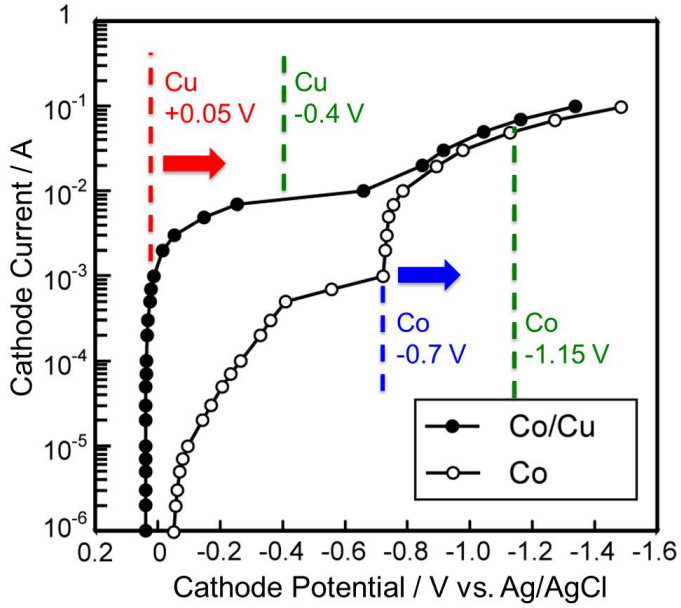

Figure 16. Cathode polarization curves for electrodeposition of Cu and Co from the mixed solution (containing Cu^{2+} and Co^{2+} ions) and the solution containing only Co^{2+} ions.

Growth rates of nanowires were estimated by the channel filling time, which was determined from the time dependence of deposition current at each potential. Figure 17 shows the effect of cathode potential on the time dependence of cathodic current during the elec-

http://dx.doi.org/10.5772/3367

trodeposition of Co nanowires. The cathode potentials were fixed to -0.80,-0.85, -0.90, -0.95 and -1.0 V. To determine the nanowire growth rate, the channel-filling time was estimated by monitoring the deposition current. When the nanowires reach the membrane surface, the current will increase drastically due to the formation of hemispherical caps. The growth rates were calculated dividing the channel length by the channel-filling time. For example, at –1.0 V, the channel-filling time is around 40 s and the deposition rate is estimated to be ca. 150nm/s. On the basis of the results shown in Figure 16 and Figure 17, the optimum deposition potentials of Cu and Co are determined to be about –0.4 and –1.15 V (vs. Ag/AgCl) which is the potential region nobler than the diffusion limit potential of each metal ion. Typical deposition rates of Cu and Co were roughly 10 nm/s (at –0.4 V) and 200 nm s^{-1} (at –1.15 V).

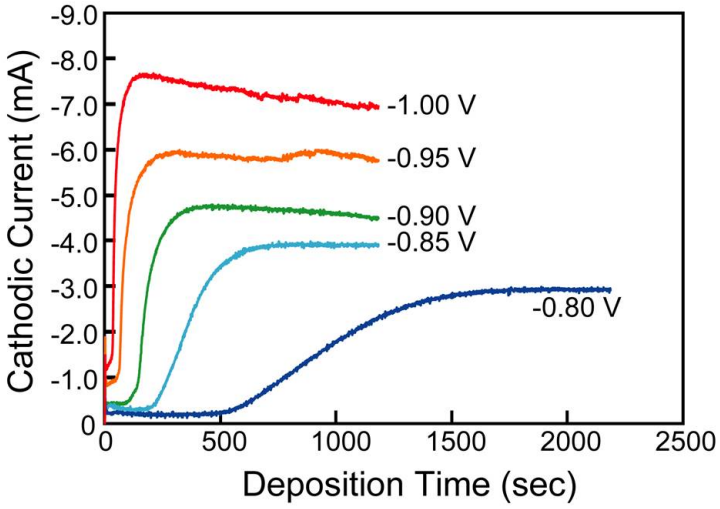

Figure 17. Effect of cathode potential on the time dependence of cathodic current during the electrodeposition of Co nanowires.

Co/Cu multilayered nanowires were synthesized alternatingly switching cathode potential from -0.4 V (for Cu layer) to -1.15 V (for Co layer) as shown in Figure 18. According to this figure, when the potential is switched from -1.15 V to -0.4 V, anodic current is observed. This is resulting from the dissolution of electrodeposited Co, because -0.4V is more nobler than the equilibrium potential of Co. At this potential, it is estimated that the Cu deposition and Co dissolution will proceed simultaneously. According to the time-dependence of cathodic current during electrodeposition of Co/Cu multilayered nanowires as shown in Figure 19, filling time was around 3500 s and the deposition rate was estimated to be about 17 nm/s.

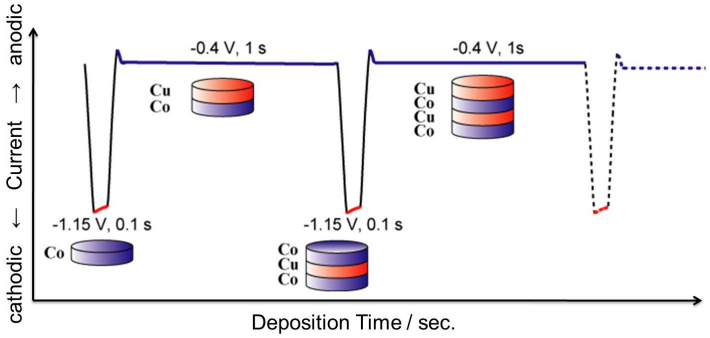

Figure 18. Growing process of Co/Cu multilayered nanowires synthesized alternatingly switching cathode potential from -0.4 V (for Cu layer) to -1.15 V (for Co layer).

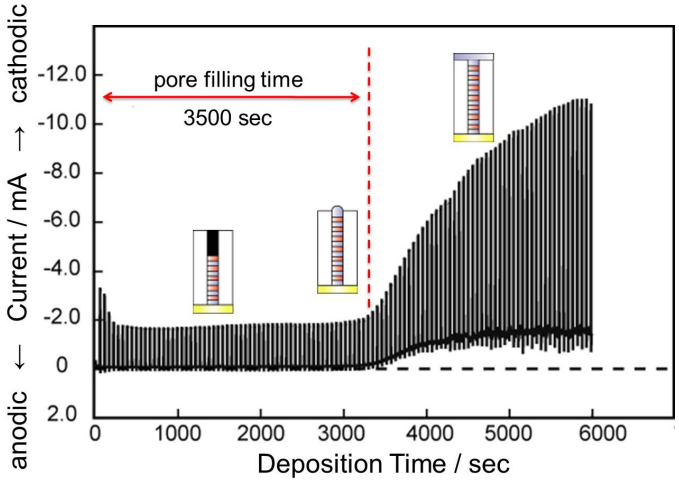

Figure 19. Time dependence of observed-current during the electrodeposition of Co/Cu multilayered nanowires.

4.2. Structure of Co/Cu Multilayered Nanowires

TEM bright field images of electrodeposited Co/Cu multilayered nanowires were investigated as shown in Figure 20. Shape of the nanowires was almost cylindrical and the multilayered structure was also observed as shown in this images. In the structure, several stacking faults were also observed. There would be significant strain energy in the interphase boundary between Co and Cu layer. The strain energy could be stored as the stacking fault energy. It is well known that the stacking fault structure is usually observed in fcc crystals such

http://dx.doi.org/10.5772/3367

as Au, Ag, Cu, Ni, Al, etc. Therefore, the stacking fault structure would be introduced to the Cu layer from the interface between Co and Cu layer.

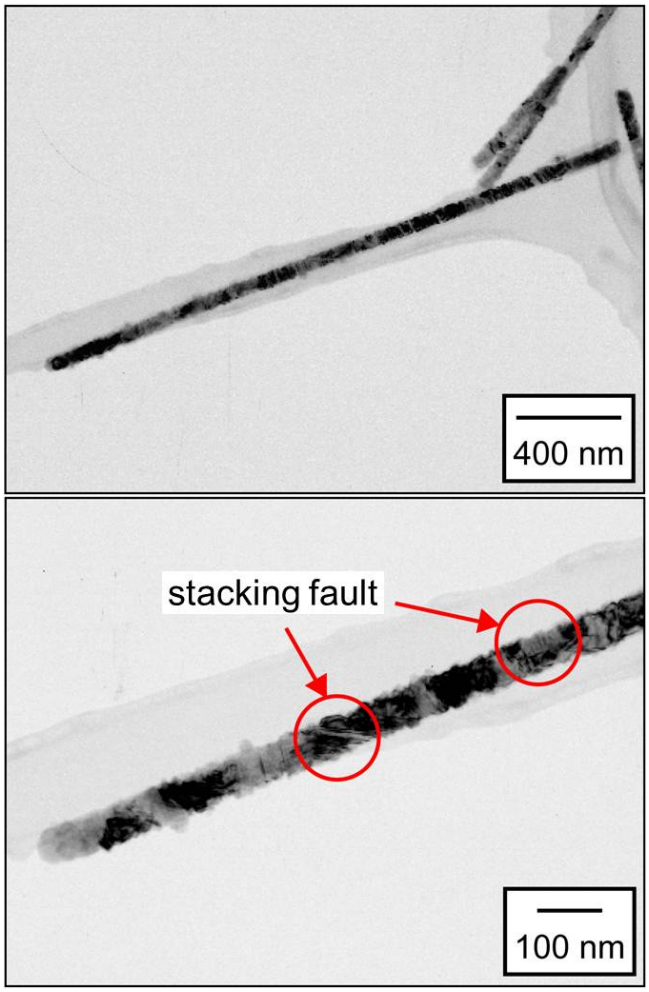

Figure 20. TEM bright field images of Co/Cu multilayered nanowires electrodeposited in nano-channel membrane filters.

4.3. Magnetic Properties of Co/Cu Multilayered Nanowires

Typical perpendicular magnetization behavior was observed from the magnetic hysteresis loops of electrodeposited Co/Cu multilayered nanowires with diameter of 60 nm and length of 60μm as shown in Figure 21-(a). Coercive force of Co/Cu multilayered nanowires was ca.

1 kOe. This is resulting from the shape anisotropy of nanowires with super large aspect ratio of ca. 1000. The magnetoresistance curves revealed that 10.5 % of GMR effect was obtained in the multilayered nanowires with Co layer 10nm, Cu layer 10 nm and 3000 bi-layers as shown in Figure 21-(b).

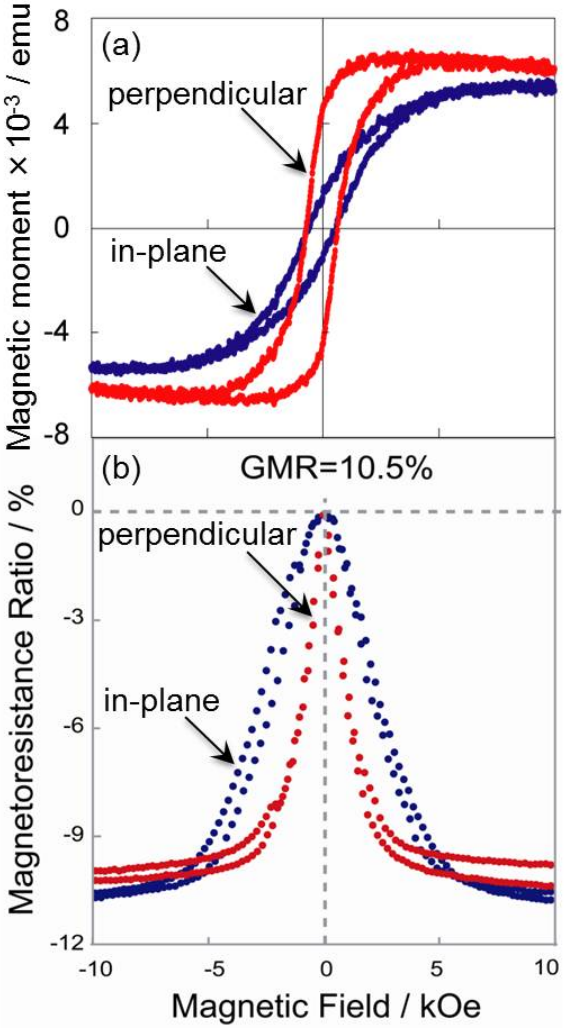

Figure 21. Magnetic hysteresis loops (a) and magnetoresistance curves (b) of Co/Cu multilayered nanowires electrodeposited into anodized aluminum oxide templates with channel-diameter of 60 nm. Magnetic field was applied to in-plan direction and perpendicular direction to the membrane film plan. The perpendicular direction to the membrane film plan corresponds to the parallel direction to the long axis of nanowires.

5. Summary

Anodized aluminum oxide films with the thickness ranging from 2μm to 200 μm were synthesized using a bipolar continuous electrolysis process with anodic oxidation and cathodic exfoliation as well as barrier layer thinning process using chemical etching technique. 3.2 % of AMR effect was observed in Ni-1.5at.% Co alloy nanowires with diameter of 60 nm and length of 60μm. Co/Cu multilayered nanowires with Co-10 nm, Cu-10 nm and 3000 bi-layers were synthesized using a pulsed current electrodeposition technique. 10.5 % of GMR effect was observed in Co/Cu multilayered nanowires electrodeposited into anodized aluminum oxide template with super large aspect ratio of ca. 1000.

Author details

Takeshi Ohgai*

Address all correspondence to: ohgai@nagasaki-u.ac.jp

Division of Chemistry and Materials Science, Nagasaki University, 1-14 Bunkyo-machi, Nagasaki 852-8521, Japan

References

[1] Goad, D. G. W., & Moskovits, M. (1978). Colloidal Metal in Aluminum-oxide. *Journal of Applied Physics*, 49(5), 2929-2934.

[2] Forrer, P., Schlottig, F., Siegenthaler, H., & Textor, M. (2000). Electrochemical Preparation and Surface Properties of Gold Nanowire Arrays Formed by the Template Technique. *Journalof Applied Electrochemistry*, 30(5), 533-541.

[3] Sauer, G., Brehm, G., Schneider, S., Nielsch, K., Wehrspohn, R. B., Choi, J., Hofmeister, H., & Gösele, U. (2002). Highly Ordered Monocrystalline Silver Nanowire Arrays. *Journal of Applied Physics*, 91(5), 3243-3247.

[4] Wang, W., Huang, Q., Jia, F., & Zhu, J. (2004). Electrochemically Assembled p-type Bi_2Te_3Nanowire Arrays. *Journal of Applied Physics*, 96(1), 615-618.

[5] Oh, J., Tak, Y., & Lee, J. (2004). Electrodeposition of Cu_2O Nanowires Using Nanoporous Alumina Template. *Electrochemical and Solid-State Letters* , C 27-C30.

[6] Zhang, X., Hao, Y., Meng, G., & Zhang, L. (2005). Fabrication of Highly Ordered InSb Nanowire Arrays by Electrodeposition in Porous Anodic Alumina Membranes. *Journal ofThe Electrochemical Society*, 152(10), C664-C668.

[7] Ohgai, T., Gravier, L., Hoffer, X., & Ansermet, J. P. (2005). CdTe Semiconductor Nanowires and NiFe Ferro-magnetic Metal Nanowires Electrodeposited into Cylin-

drical Nano-pores on the Surface of Anodized Aluminum. *Journalof Applied Electrochemistry*, 35(5), 479-485.

[8] Katkar, R. A., & Tait, G. B. (2007). The Effect of Stationary Ultraviolet Excitation on the Optical Properties of Electrochemically Self-assembled Semiconductor Nanowires. *Journal of Applied Physics*, 101(5), 053508.

[9] Inguanta, R., Sunseri, C., & Piazza, S. (2007). Photoelectrochemical Characterization of Cu_2O-Nanowire Arrays Electrodeposited into Anodic Alumina Membranes. Electrochemical and Solid-State Letters ., 10(12), K63-K66.

[10] Kim, D. J., Seol, J. K., Lee, M. R., Hyung, J. H., Kim, G. S., Ohgai, T., & Lee, S. K. (2012). Ferromagnetic Nickel Silicide Nanowires for Isolating Primary $CD4^+$ T Lymphocytes. *Applied Physics Letters*.

[11] Martin, C. R. (1991). Template Synthesis of Polymeric and Metal Microtubules. *Advanced Materials*, 3(9), 457-459.

[12] Spohr, R., Zet, C., Fischer, B. E., Kiesewetter, H., Apel, P., Gunko, I., Ohgai, T., & Westerberg, L. (2010). Controlled Fabrication of Ion Track Nanowires and Channels. *Nuclear Instruments and Methods in Physics Research B*, 268(6), 676-686.

[13] Whitney, T. M., Jiang, J. S., Searson, P. C., & Chien, C. L. (1993). Fabrication and Magnetic Properties of Arrays of Metallic Nanowires. *Science*, 261(5126), 1316-1319.

[14] Piraux, L., George, J. M., Despres, J. F., Leroy, C., Ferain, E., Legras, R., Ounadjela, K., & Fert, A. (1994). Giant Magnetoresistance in Magnetic Multilayered Nanowires. *Applied Physics Letters*, 65(19), 484-486.

[15] Blondel, A., Meier, J. P., Doudin, B., & Ansermet, J. P. (1994). Giant Magnetoresistance of Nanowires of Multilayers. *Applied Physics Letters*, 65(23), 3019-3021.

[16] Ohgai, T., Enculescu, I., Zet, C., Westerberg, L., Hjort, K., Spohr, R., & Neumann, R. (2006). Magneto-sensitive Nickel Nanowires Fabricated by Electrodeposition into Multi- and Single-ion Track Templates. *Journalof Applied Electrochemistry*, 36(10), 1157-1162.

[17] Ohgai, T., Hjort, K., Spohr, R., & Neumann, R. (2008). Electrodeposition of Cobalt Based Ferromagnetic Metal Nanowires in Polycarbonate Films with Cylindrical Nanochannels Fabricated by Heavy-ion-track Etching. *Journalof Applied Electrochemistry*, 38(5), 713-719.

[18] Kawai, S., & Ueda, R. (1975). Magnetic Properties of Anodic Oxide Coatings on Aluminum Containing Electrodeposited Co and Co-Ni. *Journal ofThe Electrochemical Society*, 122(1), 32-36.

[19] Kawai, S. (1975). Retentivities of Anodic Oxide Coatings on Aluminum Containing Electrodeposited Cobalt, Nickel, and Cobalt-Nickel. *Journal ofThe Electrochemical Society*, 122(8), 1026-1029.

[20] Kawai, S., & Ishiguro, I. (1976). Recording Characteristics of Anodic Oxide Films on Aluminum Containing Electrodeposited Ferromagnetic Metals and Alloys. *Journal ofThe Electrochemical Society*, 123(7), 1047-1051.

[21] Tsuya, N., Saito, Y., Nakamura, H., Hayano, S., Furugohri, A., Ohta, K., Wakui, Y., & Tokushima, T. A. (1986). Perpendicular Magnetic Recording Medium by Alumite. *Journal of Magnetism and Magnetic Materials*, 54-57(3), 1681-1682.

[22] Tsuya, N., Tokushima, T., Shiraki, M., Wakui, Y., Saito, Y., Nakamura, H., & Katsumata, Y. (1987). Magnetic Alumite Disc for Perpendicular Recording. *IEEE Transactions on Magnetics*, 23(1), 53-55.

[23] Huysmans, G. T. A., Lodder, J. C., & Wakui, J. (1988). Magnetization Curling in Perpendicular Iron Particle Arrays (Alumite Media). *Journal of Applied Physics*, 64(4), 2016-2021.

[24] Cheng, T. J., Jorné, J., & Gau, J. S. (1990). Magnetic Anisotropy of Electrodeposited Cobalt on Alumite Substrate. *Journal ofThe Electrochemical Society*, 137(1), 93-95.

[25] Zhang, L. C., & Lodder, J. C. (1990). The Influence of the Packing Density on the Magnetic Behaviour of Alumite Media. Journal of Magnetism and Magnetic Materials; , 88(1-2), 2236-2246.

[26] Al, Mawlawi. D., Coombs, N., & Moskovits, M. (1991). Magnetic Properties of Fe Deposited into Anodic Aluminum Oxide Pores as a Function of Particle Size. *Journal of Applied Physics*, 70(8), 4421-4425.

[27] Nielsch, K., Müller, F., Li, A. P., & Gösele, U. (2000). Uniform Nickel Deposition into Ordered Alumina Pores by Pulsed Electrodeposition. *Advanced Materials*, 12(8), 582-586.

[28] Evans, P. R., Yi, G., & Schwarzacher, W. (2000). Current Perpendicular to Plane Giant Magnetoresistance of Multilayered Nanowires Electrodeposited in Anodic Aluminum Oxide Membranes. *Applied Physics Letters*, 76(4), 481-483.

[29] Ohgai, T., Hoffer, X., Gravier, L., Wegrowe, J. E., & Ansermet, J. P. (2003). Bridging the Gap Between Template Synthesis and Microelectronics: Spin-Valves and Multilayers in Self-organized Anodized Aluminum Nanopores. *Nanotechnology*, 14(9), 978-982.

[30] Ohgai, T., Hoffer, X., Fabian, A., Gravier, L., & Ansermet, J. P. (2003). Electrochemical Synthesis and Magnetoresistance Properties of Ni, Co and Co/Cu Nanowires in Nano-porous Anodic Oxide Layer on Metallic Aluminum. *Journal of Materials Chemistry*, 13(10), 2530-2534.

[31] Ohgai, T., Gravier, L., Hoffer, X., Lindeberg, M., Hjort, K., Spohr, R., & Ansermet, J. P. (2003). Template Synthesis and Magnetoresistance Property of Ni and Co Single Nanowires Electrodeposited into Nano-pores with Wide Range of Aspect Ratios. *Journal of Physics D: Applied Physics*, 36(24), 3109-3114.

[32] Ohgai, T., Hoffer, X., Gravier, L., & Ansermet, J. P. (2004). Electrochemical Surface Modification of Aluminum Sheets for Application to Nanoelectronic Devices: Anodization Aluminum and Electrodeposition of Cobalt-Copper. *Journalof Applied Electrochemistry*, 34(10), 1007-1012.

[33] Wu, M. T., Leu, I. C., Yen, J. H., & Hon, M. H. (2004). Preparation of Ni Nanodot and Nanowire Arrays Using Porous Alumina on Silicon as a Template without a Conductive Interlayer. *Electrochemical and Solid-State Letters*, 7(5), C61-C63.

[34] Chu, S. Z., Inoue, S., Wada, K., Kanke, Y., & Kurashima, K. (2005). Fabrication and Characterization of Integrated Ultrahigh-density Fe-Pt Alloy Nanowire Arrays on Glass. *Journal ofThe Electrochemical Society*, 152(1), C42-C47.

[35] Wang, X. W., Fei, G. T., Chen, L., X.u, X. J., & Zhang, L. D. (2007). Orientation-controllable Growth of Ni Nanowire Arrays with Different Diameters. *Electrochemical and Solid-State Letters*, 10(4), E 1-E3.

[36] Friedman, A. L., & Menon, L. (2007). Optimal Parameters for Synthesis of Magnetic Nanowires in Porous Alumina Templates. *Journal ofThe Electrochemical Society*, 154(4), E 68-E70.

[37] Li, F., & Metzger, R. M. (1997). Activation Volume of α-Fe Particles in Alumite Films. *Journal of Applied Physics*, 81(8), 3806-3808.

[38] Zeng, H., Zheng, M., Skomski, R., Sellmyer, D. J., Liu, Y., Menon, L., & Bandyopadhyay, S. (2000). Magnetic Properties of Self-assembled Co Nanowires of Varying Length and Diameter. *Journal of Applied Physics*, 87(9), 4718-4720.

[39] Peng, Y., Zhang, H. L., Pan, S. L., & Li, H. L. (2000). Magnetic Properties and Magnetization Reversal of α-Fe Nanowires Deposited in Alumina Film. *Journal of Applied Physics*, 87(10), 7405-7408.

[40] Yin, A. J., Li, J., Jian, W., Bennett, A. J., & Xu, J. M. (2001). Fabrication of Highly Ordered Metallic Nanowire Arrays by Electrodeposition. *Applied Physics Letters*, 79(7), 1039-1041.

[41] Masuda, H., & Fukuda, K. (1995). Ordered Metal Nanohole Arrays Made by a Two-Step Replication of Honeycomb Structures of Anodic Alumina. *Science*, 268(5216), 1466-1468.

[42] Masuda, H., & Satoh, M. (1996). Fabrication of Gold Nanodot Array Using Anodic Porous Alumina as an Evaporation Mask. *Japanese Journal of Applied Physics*, 35, L126-L129.

[43] Masuda, H., Yamada, H., Satoh, M., Asoh, H., Nakao, M., & Tamamura, T. (1997). Highly Ordered Nanochannel-array Architecture in Anodic Alumina. *Applied Physics Letters*, 71(19), 2770-2772.

[44] Jessensky, O., Müller, F., & Gösele, U. (1998). Self-organized Formation of Hexagonal Pore Arrays in Anodic Alumina. *Applied Physics Letters*, 72(10), 1173-1175.

http://dx.doi.org/10.5772/3367

[45] Li, A. P., Müller, F., Birner, A., Nielsch, K., & Gösele, U. (1998). Hexagonal Pore Arrays with a 50-420 nm Interpore Distance Formed by Self-organization in Anodic Alumina. *Journal of Applied Physics*, 84(11), 6023-6026.

[46] Tayaoka, A., Tayaoka, E., & Yamasaki, J. (1996). Preparation of Co-Fe-P Amorphous Fine Needles with Anodization Technique and Measurement of Demagnetizing Factor. *Journal of Applied Physics*, 79(8), 6016-6018.

[47] Ferre, R., Ounadjela, K., George, J. M., Piraux, L., & Dubois, S. (1997). Magnetization Processes in Nickel and Cobalt Electrodeposited Nanowires. *Physical Review B*, 56(21), 14066 .